Available online at www.sciencedirect.com
SCIENCE DIRECT®
PERGAMON
International Journal of Heat and Mass Transfer 46 (2003) 3605–3617
International Journal of HEAT and MASS TRANSFER
www.elsevier.com/locate/ijhmt

Transient buoyant convection of a power-law non-Newtonian fluid in an enclosure

Gi Bin Kim [a], Jae Min Hyun [a,*], Ho Sang Kwak [b]

[a] Department of Mechanical Engineering, Korea Advanced Institute of Science and Technology, 373-1 Kusong-dong, Yusong-gu, Taejon 305-701, South Korea

[b] School of Mechanical Engineering, Kumoh National University of Technology, 188 Shinpyung-dong, Kumi, Kyongbuk 730-701, South Korea

Received 6 May 2002; received in revised form 15 March 2003

Abstract

Transient buoyant convection in a square enclosure of a non-Newtonian fluid is studied. A simple power-law fluid model, with the power-law index n and the consistency coefficient K, is adopted. Flow is initiated from the motionless isothermal initial state by abruptly raising the temperature at one vertical sidewall and lowering the temperature at the opposite vertical sidewall. The appropriately defined overall Rayleigh number Ra is large to render a boundary layer-type flow. A scale analysis is performed to gain a rudimentary understanding of the evolution process. Principal force balances are considered in each of the transient stages. Comprehensive numerical solutions are acquired to the governing equations. The transient flow and thermal characteristics, both in the boundary layers and in the interior, are portrayed. The effects of Ra and of n on the behavior of the Nusselt number are delineated. The system-wide heat transport at the steady state is calculated. Based on the numerical results, the Nusselt number correlations are proposed. The numerical solutions are in broad qualitative agreement with the descriptions obtainable from the scale analysis.

1. Introduction

Transient buoyant convection in an enclosed space, under various thermal and mechanical forcings, has been extensively studied [1]. The convective flow and heat transfer characteristics pertinent to the geometrical and dynamical constraints have been documented. For most applications, the overall Rayleigh number is large, and rectangular cavities of aspect ratio O(1) have been dealt with. One prominent flow layout is due to Patterson and Imberger [2], which is hereafter referred to as P & I. This model delineated the transient evolution from the motionless isothermal initial state to the final state. The flow is initiated by abruptly raising the temperature at one vertical sidewall and simultaneously lowering the temperature at the opposite vertical sidewall. Several relevant time scales and the evolution scenarios, together with the characterization of transient heat transport, have been brought forth.

It is emphasized that the majority of existing studies have been concerned with the Newtonian fluids. Despite the obvious relevance to industrial applications, little has been reported on buoyant convection involving non-Newtonian fluids. The free convection of a non-Newtonian fluid over a heated plate and a cylindrical enclosure has received some attention [3–11]. The methodologies encompassed analytical [3], numerical [4] and experimental [5] techniques, and the results established that the free convection features are substantially affected by the rheological properties of the fluid. However, the crucial issue of the time-dependent buoyant convective process in an enclosure of a non-Newtonian fluid has remained largely unexplored. For the steady convection of an enclosed non-Newtonian fluid, the prior works addressed the problem of buoyant convection in a porous cavity [12–14]. The purpose of the present paper is to portray the principal aspects of

* Corresponding author. Tel.: +82-42-869-3012; fax: +82-42-869-3210.
E-mail address: jmhyun@cais.kaist.ac.kr (J. Min Hyun).

0017-9310/03/$ - see front matter © 2003 Elsevier Ltd. All rights reserved.
doi:10.1016/S0017-9310(03)00149-2

Nomenclature

Ar	cavity aspect ratio, H/L
Nu	overall Nusselt number, Eq. (25)
g	gravitational acceleration
H	height of the cavity
K	consistency coefficient, Eq. (6)
L	width of the cavity
n	power-law index, Eq. (6)
p, P	dimensional and non-dimensional pressure
Pr	system-wide Prandtl number, Eq. (10a)
Ra	system-wide Rayleigh number, Eq. (10b)
T	dimensional temperature
t	dimensional time
t_B	formation time scale of the vertical boundary layer, Eq. (11a)
t_C	heat-up or convective time scale, Eq. (17)
t_D	diffusion time scale, Eq. (19)
t_G	period of internal gravity oscillation, Eq. (18)
t_H	arrival time scale of viscous intrusion at opposite wall, Eq. (15)
u, v	dimensional velocity components in the x and y directions
x, y	dimensional horizontal and vertical coordinates
U, V	dimensionless velocity components in the X and Y directions
X, Y	dimensionless horizontal and vertical coordinates
v_V	velocity scale of vertical boundary layer, Eq. (11b)
v_H	velocity scale of viscous horizontal intrusion layer, Eq. (16)

Greek symbols

β	isobaric coefficient of volumetric thermal expansion
δ_H	thickness of horizontal viscous intrusion layer, Eq. (14)
δ_V	thickness of outer viscous layer, Eq. (11d)
δ_T	thickness of vertical thermal boundary layer, Eq. (11c)
κ	thermal diffusivity
μ	dynamic viscosity
θ	non-dimensional temperature
τ	non-dimensional time
$\Delta\tau$	time increment for numerical computations
ΔT	temperature difference between vertical sidewalls
ψ	non-dimensional stream function

Subscripts

0	reference condition at $T = T_0$
C	cold sidewall
H	hot sidewall
ss	steady state
a	apparent viscosity

Superscript

$*$	dimensionless viscosity

the transient process of a non-Newtonian clear fluid in the flow configuration of P & I.

In order to gain basic physical understandings, the non-Newtonian fluid considered in this study is assumed to follow the well-known power-law model [3–10]. An order-of-magnitude analysis is carried out to depict the transient stages. The bulk of the present effort is directed to obtaining comprehensive and detailed numerical solutions. Emphasis is given to the specific influences of the rheological properties of the fluid. The flow and heat transfer characteristics at the final state will also be scrutinized, and comparisons with those of a Newtonian fluid will be made.

2. Mathematical formulation

Consider a two-dimensional closed rectangular cavity of length L and height H, which is filled with an incompressible non-Newtonian fluid. As displayed in Fig. 1, the fluid is initially isothermal (temperature T_0) and at rest. The top and bottom horizontal endwalls are thermally insulated. At time $t = 0$, the left- and

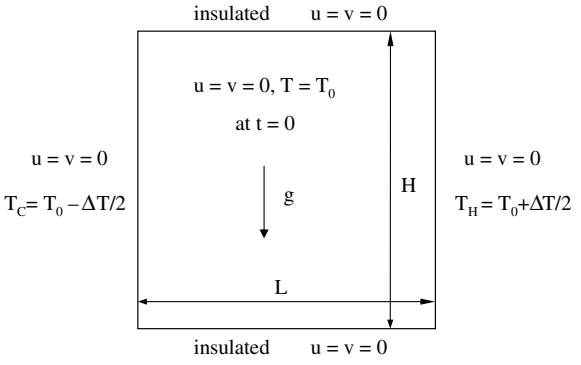

Fig. 1. Schematics of flow configuration.

right-sidewalls are instantaneously cooled and heated respectively to temperatures $T_0 - \Delta T/2$ and $T_0 + \Delta T/2$, and these thermal boundary conditions are maintained thereafter. The subsequent fluid motion is governed by the time-dependent Cauchy equations. With the invocation of the Boussinesq-fluid approximation, i.e., $\rho = \rho_0[1 - \beta(T - T_0)]$, these are [3,6,10]

$$\frac{\partial u}{\partial x} + \frac{\partial v}{\partial y} = 0, \tag{1}$$

$$\frac{\partial u}{\partial t} + u\frac{\partial u}{\partial x} + v\frac{\partial u}{\partial y} = -\frac{1}{\rho_0}\frac{\partial p}{\partial x} + \frac{1}{\rho_0}\left(\frac{\partial \tau_{xx}}{\partial x} + \frac{\partial \tau_{xy}}{\partial y}\right), \tag{2}$$

$$\frac{\partial v}{\partial t} + u\frac{\partial v}{\partial x} + v\frac{\partial v}{\partial y} = -\frac{1}{\rho_0}\frac{\partial p}{\partial y} + \frac{1}{\rho_0}\left(\frac{\partial \tau_{xy}}{\partial x} + \frac{\partial \tau_{yy}}{\partial y}\right) + g\beta(T - T_0), \tag{3}$$

$$\frac{\partial T}{\partial t} + u\frac{\partial T}{\partial x} + v\frac{\partial T}{\partial y} = \kappa\left(\frac{\partial^2 T}{\partial x^2} + \frac{\partial^2 T}{\partial y^2}\right). \tag{4}$$

In the above, (u, v) represent the velocity components in the horizontal (x) and vertical (y) directions; t the time; T the temperature; p the pressure; g the gravitational acceleration; and ρ, β, and κ the density, coefficient of thermometric expansion, and thermal diffusivity of the fluid at temperature T_0.

The associated initial and boundary conditions are

$$u = v = 0, \quad T = T_0 \quad t < 0; \tag{5}$$

$$u = v = 0 \quad \text{at } x = 0, L, \quad \text{and} \quad y = 0, H;$$

$$\frac{\partial T}{\partial y} = 0 \quad \text{at } y = 0, H;$$

$$T = T_0 \mp \Delta T/2 \quad \text{at } x = 0, L, \quad t > 0.$$

The essential part of the formulation is to adopt a suitable constitutive equation, which relates the individual components of the stress tensor to the relevant kinematic variables. For this purpose, a purely-viscous non-Newtonian fluid is considered, which follows the Ostwald–De Waele power-law [3–10]:

$$\tau_{ij} = 2\mu_a D_{ij} = 2K(2D_{kl}D_{kl})^{(n-1)/2}D_{ij}. \tag{6}$$

The above representation involves two material parameters, i.e., K, the consistency coefficient; and n, the power-law index, and D_{ij} indicates the rate-of-deformation tensor. Obviously, the usual Newtonian fluid corresponds to the case $n = 1$ with the coefficient of viscosity K; whereas the case $n > 1$ describes the dilatant (or shear-thickening) behavior, and $n < 1$ denotes the pseudoplastic (or shear-thinning) behavior of a non-Newtonian fluid.

Here, the limitation of the power-law model in Eq. (6) is briefly stated. As is generally known, this model for pseudoplastic fluids predicts an infinite viscosity at the limit of zero shear rate, whereas the viscosity of all real non-Newtonian fluids exhibits a Newtonian behavior at low shear rates. In the present problem, this situation would occur in the enclosure, especially, at the beginning of the transient period motionless state. To eliminate the singularity associated with the infinite viscosity in the numerical computations, various values of a zero shear-rate viscosity in the numerical computations were tested, and these effects on the major transient phenomena were negligible. The pseudoplastic fluids have generally a high viscosity, and the variation in the viscosity due to temperature change has also a direct impact on the thermal and flow fields. However, when the variation in the temperature is not large, the variation in the viscosity is also small. In the present set-up, the dependency of K on temperature is not considered; a small temperature difference ΔT is assumed. For detailed rheological aspects, the reader is referred to the more specialized treatments.

For the two-dimensional Cartesian coordinates, D_{ij} in Eq. (6) simplifies to

$$D_{ij} = \frac{1}{2}\left(\frac{\partial u_i}{\partial x_j} + \frac{\partial u_j}{\partial x_i}\right). \tag{7}$$

From Eqs. (6) and (7), the apparent viscosity μ_a is derived:

$$\mu_a = K\left\{2\left[\left(\frac{\partial u}{\partial x}\right)^2 + \left(\frac{\partial v}{\partial y}\right)^2\right] + \left(\frac{\partial v}{\partial x} + \frac{\partial u}{\partial y}\right)^2\right\}^{(n-1)/2}. \tag{8}$$

Clearly, for a Newtonian fluid ($n = 1$), μ_a [$= K$] reduces to the conventional viscosity. However, for a non-Newtonian fluid, μ_a shows more complex dependence on the fluid property and flow variables. Therefore, there arises a need to introduce and utilize a physical quantity with the dimension of $(\text{length})^2(\text{time})^{-1}$, which would play a role analogous to the kinematic viscosity of a Newtonian fluid. The introduction of such a quantity for a non-Newtonian fluid will facilitate the interpretation of the flow features, in parallel with the concepts and tools that are effective for a Newtonian fluid. Also, by using such a quantity, consistent definitions of the dimensionless parameters, which are characteristic of the system-wide global heat transports, can be achieved. In the literature, searches for the proper combinations of flow variables have been made, both for a free convection about a flat plate [3–10] and for a porous cavity [12–14]. Based on the physical rationalizations and trial-and-error efforts, a grouping, which consists of the consistency coefficient K, the power-law index n, the fluid density ρ_0 and the cavity height H, emerges to be appropriate [5];

$$v' \equiv \left(\frac{K}{\rho_0}\right)^{1/(2-n)} H^{2(1-n)/(2-n)}. \tag{9}$$

Note that the role of v', of which the dimension is $m^2\,s^{-1}$, is analogous to that of the kinematic viscosity of a Newtonian fluid. By using v', the Prandtl (Pr) and Rayleigh (Ra) numbers are defined

$$Pr \equiv \frac{(K/\rho_0)^{1/(2-n)} H^{2(1-n)/(2-n)}}{\kappa} \tag{10a}$$

and

$$Ra \equiv \frac{g\beta\Delta T H^3}{\kappa (K/\rho_0)^{1/(2-n)} H^{2(1-n)/(2-n)}}. \tag{10b}$$

The use of the above-mentioned v' was proposed and refined in the preceding numerical and experimental endeavors [5,6,10].

3. Scale analysis

In line with the undertaking of P & I, a scale analysis is carried out to acquire a rudimentary picture.

3.1. Growth of the vertical thermal boundary layers

Immediately after the impulsive imposition of the differential heating at the sidewalls, the scales for time, velocity and length for the growth of the vertical thermal boundary layer, under the assumption of viscous-buoyancy force balance, are, respectively:

$$t_B \sim \frac{H^2}{\kappa} (Ra\,Pr^{n-1})^{-2/(3n+1)}, \tag{11a}$$

$$v_V \sim \frac{\kappa}{H} (Ra\,Pr^{n-1})^{2/(3n+1)}, \tag{11b}$$

$$\delta_T \sim H (Ra\,Pr^{n-1})^{-1/(3n+1)}. \tag{11c}$$

The thickness of the outer viscous layer is scaled as

$$\delta_V \sim H\,Pr^{2-n/(n+1)} (Ra\,Pr^{n-1})^{2(2-n)/(n+1)(3n+1)}. \tag{11d}$$

It is noted that, for the assumption of a thin boundary layer ($\delta_V \ll H$) to be valid,

$$Ra > Pr^{(n+3)/2}, \tag{12a}$$

and, also, for the above-described force balance to be applicable, one has

$$Ra \lesssim Pr^{(5-n)/3(1-n)} \quad \text{for } n \lesssim 1. \tag{12b}$$

The apparent viscosity μ_a of Eq. (8) is non-dimensionalized by employing v':

$$v_a^* \equiv \frac{\mu_a}{\rho_0 v'}. \tag{13a}$$

The magnitude of v_a^* in the boundary layer can be estimated, from Eqs. (8)–(11):

$$v_a^* \sim (Ra\,Pr^{-4/3})^{3(n-1)/(3n+1)}. \tag{13b}$$

3.2. Passage of the horizontal viscous intrusion layer

After the establishment of the thermal boundary layer on the vertical sidewall, the horizontal intrusion layer begins to form and moves toward the opposite sidewall on the top and bottom horizontal endwalls. At the time instant t, if the thickness of this layer is δ, then the velocity scale is $u \sim v_V \delta_T/\delta$. The horizontal intrusion layer is driven by the buoyancy-induced horizontal pressure gradient of $O(g\beta\Delta T\delta/ut)$, which can be deduced Eq. (3). The intrusion layer grows up to a thickness $O(\delta_H)$ over the time to reach the opposite wall $t \sim L/u$. The viscous-pressure balance, from Eq. (2), gives:

$$\delta_H \sim H (Ra\,Pr^{n-1})^{-(2n+1)/2(n+1)(3n+1)} Ar^{-1/2(n+1)}, \tag{14}$$

$$t_H \sim \frac{H^2}{\kappa} (Ra\,Pr^{n-1})^{-(4n+3)/2(n+1)(3n+1)} Ar^{-(2n+3)/2(n+1)}, \tag{15}$$

and

$$v_H \sim \frac{k}{H} (Ra\,Pr^{n-1})^{(4n+3)/2(n+1)(3n+1)} Ar^{1/2(n+1)}. \tag{16}$$

3.3. Approach to the steady state (stratification of the interior core)

As succinctly portrayed in P & I, after the arrival of the horizontal intrusion at the opposite sidewall, the interior core is filled with heated (cooled) fluids by horizontal layering. This filling occurs over t_C until when all the fluids pass through the vertical thermal boundary layers,

$$t_C \sim \frac{H^2}{\kappa} (Ra\,Pr^{n-1})^{-1/(3n+1)} Ar^{-1}. \tag{17}$$

It was shown in P & I that, for a Newtonian fluid, in the convection-dominant flow regime, the size of the diffusion time scale $t_D \sim H^2/v$, relative to t_C, determines the existence of decaying wave motions; for $t_C < t_D$, the approach to the steady state is characterized by decaying internal gravity oscillations; whereas if $t_C > t_D$, the approach is monotonic [2]. The period of the system-scale internal gravity waves is expressed as [15]:

$$t_G = 2\pi \frac{(1+Ar^2)^{1/2}}{S_i N} = \frac{H^2}{\kappa} \frac{2\pi}{S_i} \left(\frac{1+Ar^2}{Ra\,Pr} \right)^{1/2}, \tag{18}$$

where $N \sim (g\beta\Delta T/H)^{1/2} \sim \kappa/H^2 (Ra\,Pr)^{1/2}$ is the Brunt-Väisälä frequency and S_i denotes the interior stratification factor $(\partial\theta/\partial Y)^{1/2}$. To estimate the time scale of t_D for a non-Newtonian fluid, the known values of the apparent viscosity (v_a) in the vertical thermal boundary

layer can be utilized. Accordingly, on this basis, the diffusive time for a non-Newtonian fluid is gauged

$$t_D \sim \frac{H^2}{\kappa}\left(Ra\,Pr^{n-1}\right)^{3-3n/(3n+1)} Pr^{n-2}. \tag{19}$$

Therefore, the criterion for the presence of transient internal waves can be stated

$$Ra > Pr^{(6-2n)/(4-3n)} Ar^{(3n+1)/(3n-4)} \quad \text{for } n < 1.0. \tag{20}$$

It is implicit in the description of the generation of wave motions that the horizontal intrusion layer transports the heat energy by convection without a significant heat loss to the core by vertical conduction [16]. This is valid if $t_H < \delta_H^2/\kappa$, or, from Eqs. (14) and (15),

$$Ra > Pr^{1-n} Ar^{-(2n+1)(3n+1)}. \tag{21}$$

Consequently, for $n < 1$ and $Ar \leqslant 1.0$, the criterion for the presence of internal wave activity may be expressed as

$$Ra > \mathrm{Max}\left(Pr^{(6-2n)/(4-3n)} Ar^{(3n+1)/(3n-4)},\ Pr^{1-n} Ar^{-(2n+1)(3n+1)}\right). \tag{22}$$

For the Newtonian fluid of $n = 1.0$, the above expression is identical with that suggested by Patterson [16].

Now, the heat transfer rate at the steady state is scrutinized. The steady Nusselt number is given by the temperature gradient across the vertical thermal boundary layer,

$$Nu_{ss} \sim \frac{L}{\Delta T}\frac{\Delta T}{\delta_T} \sim \frac{\left(Ra\,Pr^{n-1}\right)^{1/(3n+1)}}{Ar}. \tag{23}$$

This expression demonstrates that the Nusselt number is dependent on Pr and n, whereas for a Newtonian fluid with $Pr > 1.0$, this value is independent of Pr [2].

All the relevant scales discussed here are summarized at Table 1. For a Newtonian fluid ($n = 1$), these scales are reduced to the corresponding expressions stipulated by P & I [2].

4. Numerical procedure

The numerical solutions of Eqs. (1)–(5) were secured by employing a finite volume procedure, which is based on the well-established SIMPLER algorithm [21]. Spatial differencing schemes of second-order accuracy were selected for the equation terms. A central differencing was used for the diffusion terms, and the QUICK scheme [22] was employed to discretize the nonlinear convection terms. All the boundary conditions were treated by using the second-order differencing to maintain the same accuracy in the whole computation domain. To handle the nonlinearity embedded in the diffusion terms, the apparent viscosity of Eq. (8) was evaluated at the previous iteration step. Time integration was performed by using an iterative Eulerian implicit method of accuracy $O(\Delta\tau)$. Convergence of the solutions was declared at each time step when the maximum relative change between two consecutive iteration levels fell below 10^{-4} for U, V and θ. A parallel check was made to ensure that mass continuity in every computational control volume was satisfied within a relative error of 10^{-6}.

For the majority of calculations, a staggered grid with (72×72) mesh was deployed. Grid stretching was implemented to resolve thin boundary layers adjacent to the walls. A very small time step $\Delta\tau = 10^{-3} t/t_B$, i.e., 10^3 time intervals for the formation time of the vertical boundary layer, was utilized. To test the grid- and time-step independence of the solution, two additional fine meshes with different time steps were used. These

Table 1
Compilation of the relevant scales, as in Section 3

Length	δ_T	$H\left(Ra\,Pr^n - 1\right)^{-1/(3n+1)}$
	δ_V	$H\,Pr^{(2-n)/n+1}\left(Ra\,Pr^n - 1\right)^{2(2-n)/(n+1)(3n+1)}$
	δ_H	$H\left(Ra\,Pr^n - 1\right)^{-(2n+1)/2(n+1)(3n+1)} Ar^{-1/2(n+1)}$
Velocity	v_V	$\frac{\kappa}{H}\left(Ra\,Pr^n - 1\right)^{2/(3n+1)}$
	v_H	$\frac{k}{H}\left(Ra\,Pr^n - 1\right)^{(4n+3)/2(n+1)(3n+1)} Ar^{1/2(n+1)}$
Time	t_B	$\frac{H^2}{\kappa}\left(Ra\,Pr^n - 1\right)^{-2/(3n+1)}$
	t_H	$\frac{H^2}{\kappa}\left(Ra\,Pr^n - 1\right)^{-(4n+3)/2(n+1)(3n+1)} Ar^{-(2n+3)/2(n+1)}$
	t_C	$\frac{H^2}{\kappa}\left(Ra\,Pr^n - 1\right)^{-1/(3n+1)}$
	t_D	$\frac{H^2}{\kappa}\left(Ra\,Pr^n - 1\right)^{3(1-n)/(3n+1)} Pr^n - 2$
	t_G	$\frac{H^2}{\kappa}\frac{2\pi}{S_i}\left(\frac{1+Ar^2}{Ra\,Pr}\right)^{1/2}$
Apparent viscosity	v_a^*	$\left(Ra\,Pr^{-4/3}\right)^{3(n-1)/(3n+1)}$
Nusselt number at steady state	Nu_{ss}	$\frac{\left(Ra\,Pr^n - 1\right)^{1/(3n+1)}}{Ar}$

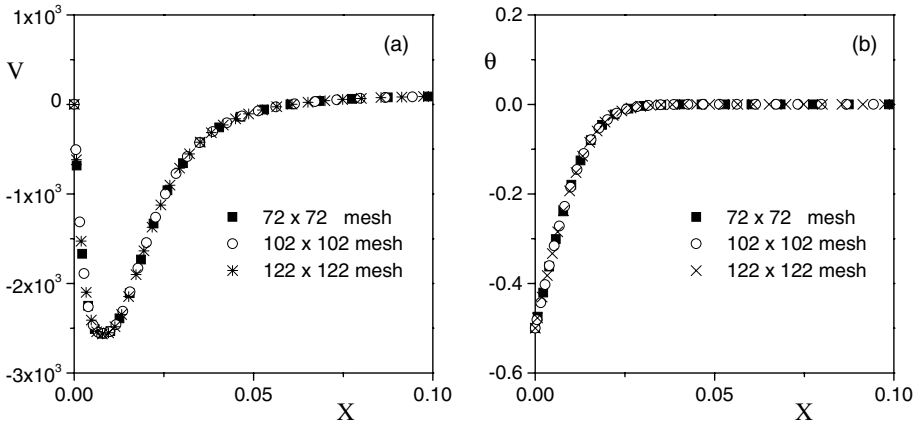

Fig. 2. Results of the grid and time-step dependency tests $Y = 0.5$, $t = 1.0t_B$, $n = 0.6$, $Ra = 10^7$, $Pr = 10^2$. (a) Vertical velocity (V); (b) temperature (θ).

Table 2
Comparison with the published results for C_{NN} for a flat plate

	Water	Carbopol 1	Carbopol 2	Carbopol 3	Carbopol 4
n	1.0	0.475	0.581	0.599	0.807
Pittman et al. (experimental)	0.61	0.49	0.50	0.58	0.64
Dale and Emery (numerical)	0.605	0.45	0.49	0.50	0.57
Tien (numerical)	0.68	0.73	0.72	0.72	0.70
Present	0.59	0.53	0.47	0.58	0.61

$Nu_x = C_{NN}(Gr_x Pr_x^n)^{1/(3n+2)}$, $q''_w = \text{const.}$

elaborate test programs demonstrated that variations between the three representations were very small, which indicated that the basic mesh of 72×72 with time-step $\Delta\tau = 10^{-3} t/t_B$ was adequate for the present task (see Fig. 2). Also, verification of the present numerical model was achieved by repeating the calculations of the published problems [2,5,17]. Table 2 illustrates the exemplary results for the free convection for a vertical plate with a constant heat flux. These comprehensive validation efforts demonstrated that the present methodologies were robust and accurate.

In the course of computations, the set of Eqs. (1)–(5) were non-dimensionalized in the following fashion:

$$\tau = \frac{t}{t_B}; \quad (X, Y) = \frac{(x, y)}{H}; \quad (U, V) = \frac{(u, v)}{\kappa/H};$$
$$P = \frac{p}{\rho_0 \kappa^2/H}; \quad \theta = \frac{T - T_0}{\Delta T}. \tag{24}$$

5. Numerical results and discussion

Results are focused to the case of weakly pseudo-plastic fluids with $0.6 \leqslant n \leqslant 1.0$, such as carboxymethyl-cellulose (CMC-series) and carboxypolymethylene (Carbopol-series) [5,10]. The aspect ratio of the enclosure was set $Ar = 1.0$, and the parameter ranges were $10^5 \leqslant Ra \leqslant 10^7$, $10^2 \leqslant Pr \leqslant 10^4$. These parameter values were chosen to exemplify practical fluids of common use in technological applications [5].

The Nusselt number at a vertical line, Nu_X, is defined as

$$Nu_X = \frac{1}{Ar} \int_0^1 \left(\frac{\partial \theta}{\partial X} - U\theta \right)_X \mathrm{d}Y. \tag{25}$$

Fig. 3 is representative of the evolution of Nu_W (at the left vertical wall, $X = 0$) and Nu_C (at the centerline, $X = 0.5$). This demonstrates a decaying oscillatory approach to the steady state of Nu_C. Fig. 3(a) is for $Ra = 10^7$, $Pr = 10^2$ and $n = 0.6$, which belongs to the oscillatory regime classified in the previous chapter. The transient flow is highly oscillatory at small and intermediate times. The oscillations are damped out at moderate and large times. At early times, there appear high-frequency oscillations in both the Nu_W and Nu_C plots. In the case of Nu_W, these are due to the passage of the perturbations in the thermal boundary layer. The short-period

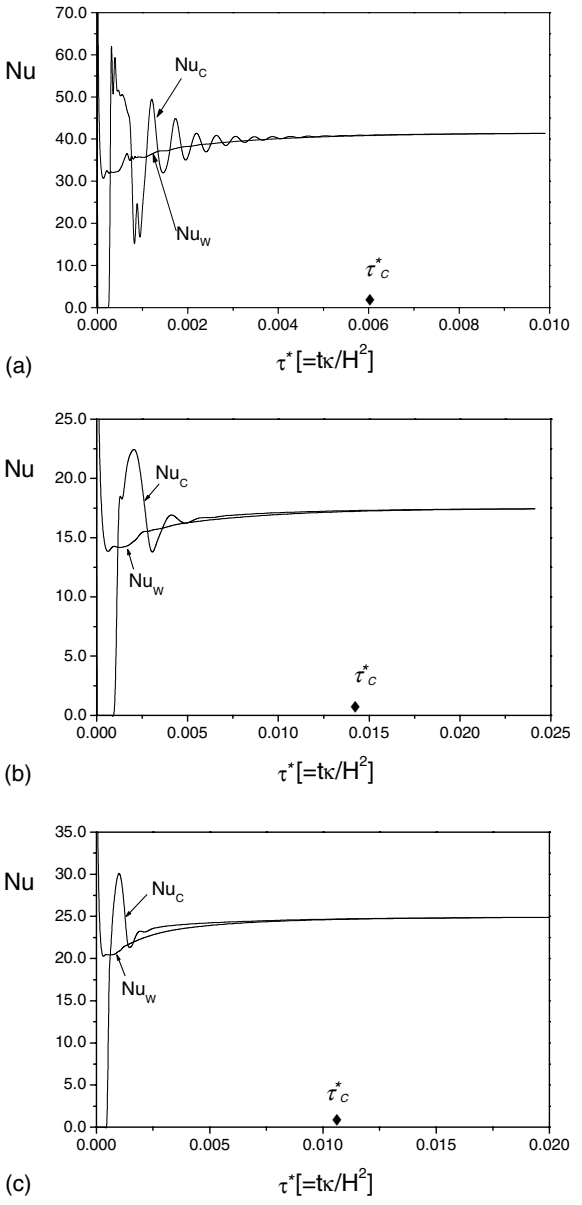

Fig. 3. Evolutions of the Nusselt numbers at the left wall, Nu_W, and at the center, Nu_C. $Pr = 10^2$. (a) $n = 0.6$, $Ra = 10^7$; (b) $n = 0.6$, $Ra = 10^6$; (c) $n = 0.8$, $Ra = 10^7$.

signals in Nu_C reflect these perturbations travelling across the horizontal intrusions [18–20]. Afterward, the decay of the cavity-scale oscillations is discernible. As *Ra* decreases or *n* increases, the oscillatory behavior is less pronounced, as shown in Fig. 3(b) and (c). The high-frequency oscillations are less visible in these cases, and the oscillatory motions decay comparatively quickly. The computed periods of oscillation in Fig. 3(a)–(c) are about 5.29×10^{-4}, 1.82×10^{-3} and 6.60×10^{-4}, respectively. The theoretical predictions for a Newtonian fluid by Eq. (18), with $S_i = 1.0$, give the periods, respectively, 8.89×10^{-4} for $Ra = 10^6$ and 2.81×10^{-4} for $Ra = 10^7$. These Newtonian-fluid predictions are slightly smaller than the computed results of Fig. 3. These discrepancies are believed to be due to the spatially non-uniform nature of the stratification ($0.5 < S_i < 1.0$) in the course of computing Eq. (18), particularly in the early part of the flow development [18]. Another feature of Fig. 3 is that the settlement to the steady state is substantially accomplished over the time scale τ^*_C. The values of τ^*_C marked in Fig. 3 are evaluated by using Eq. (17).

Fig. 4 exhibits the *Nu* results pertinent to the flow regime of monotonic approach to the steady state. The *Nu* curves tend to the steady state in a smooth and heavily damped fashion. Fig. 4(a) exemplifies the *Nu*-evolution for the representative Newtonian case ($n = 1.0$). Compared to the plots in Fig. 3 for the same *Ra* and *Pr*, the approach to the steady state in this case is monotonic (see Eq. (20)). The transient process for lower *Ra* progresses slowly. The qualitative patterns of the transient *Nu*-evolutions are largely unchanged in this parameter range. As remarked in the previous section (see Eq. (13)), the lower value of the apparent viscosity causes the effective *Ra* to increase, and, therefore, intensified convective activities are seen for low apparent viscosity. In the case of Fig. 4(d), the criterion, Eq. (20), is still satisfied. However, the value of *Ra* is relatively small so that only weak oscillations are visible. Similar results for this marginal case for a Newtonian fluid were reported in the prior work [17]. The plots displayed in Figs. 3 and 4 point to the fact that the concept of the apparent viscosity in the vertical thermal boundary layer can be applied effectively in predicting the presence of transient internal waves.

The evolutions of the transient flow and temperature fields for the oscillatory regime are exemplified in Fig. 5. These figures illustrate sequentially the formation of the vertical boundary layer, the horizontal intrusion layer and the approach to the steady state by horizontal layering. The effect of the power-law index *n* is discernible by comparing Fig. 5(a) for $n = 0.6$ and Fig. 5(b) for $n = 0.8$. The transient process for $n = 0.6$ progresses faster than for $n = 0.8$. It is informative to consult the non-dimensional time $\tau^*(\equiv tH^2/\kappa)$ in the parenthesis. Also, the vertical thermal boundary layer and the horizontal intrusion layer for $n = 0.6$ are appreciably thinner than those for $n = 0.8$. For $n = 0.6$, during the horizontal intrusion, the flow diverges ($t > t_B$), and at the intrusion nose, two distinct streams are visible: one entraining to the opposite wall across the interior, and the other forming a counterclockwise eddy in the interior. As time elapses to the instant of the first arrival of the intrusion layer at the opposite wall, the eddy formed in the departing corner has advected toward the far-away

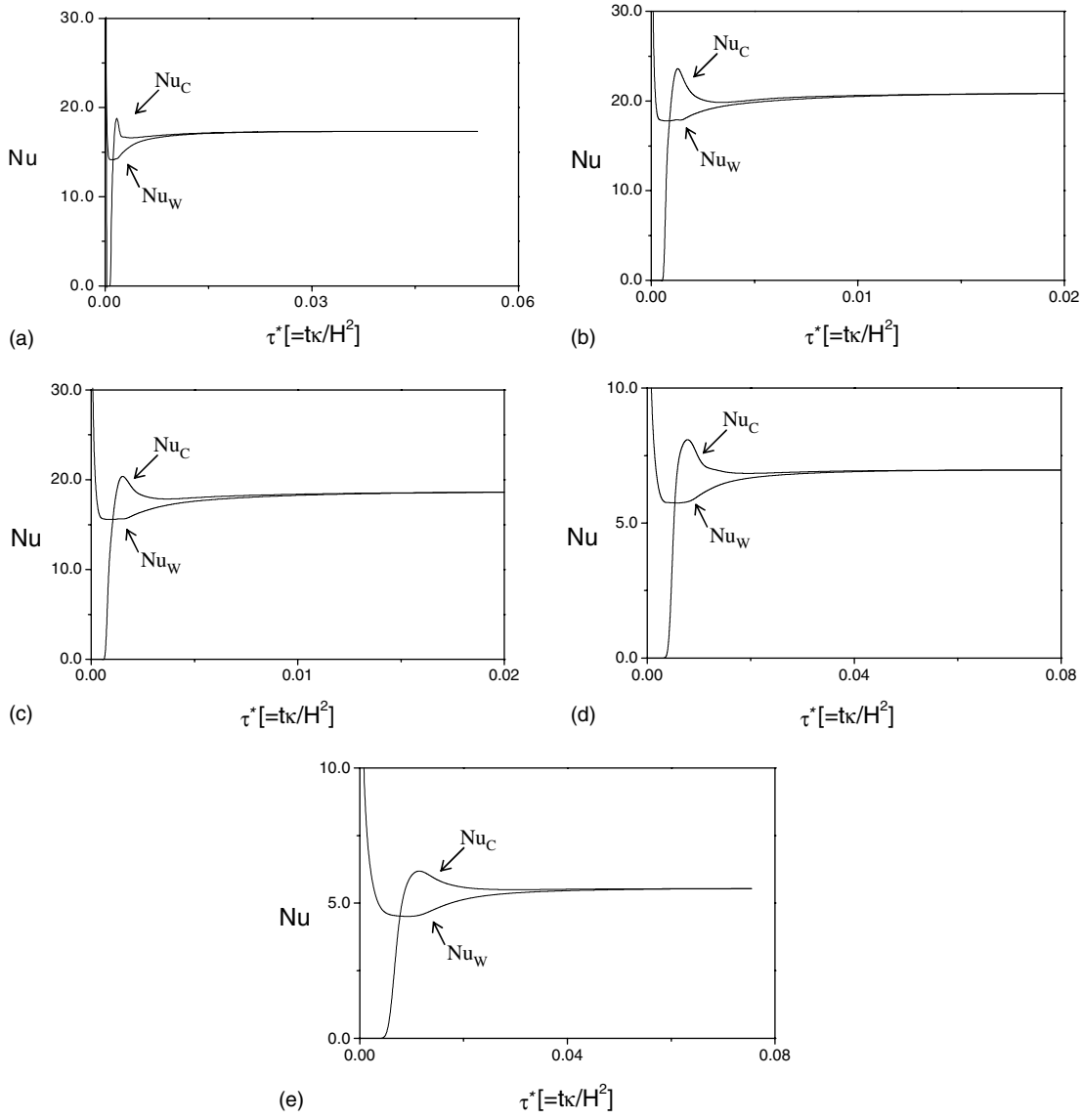

Fig. 4. Evolutions of the Nusselt numbers at the left wall, Nu_W, and at the center, Nu_C. (a) $n = 1.0$, $Ra = 10^7$, $Pr = 10^2$; (b) $n = 0.6$, $Ra = 10^7$, $Pr = 10^4$; (c) $n = 0.8$, $Ra = 10^7$, $Pr = 10^4$; (d) $n = 0.6$, $Ra = 10^5$, $Pr = 10^2$; (e) $n = 0.8$, $Ra = 10^5$, $Pr = 10^2$.

wall. The weak flow separations from the horizontal walls between the departing corner and the intrusion nose are observed ($t = 3t_H$). These are the features paradigmatic of high Ra and low Pr [18]. It is worth noting the distribution of the apparent viscosity v_a^* (see Eq. (13a)) plotted in the second column in Fig. 5(a). For a pseudo-plastic fluid ($n < 1.0$), the smallest value of the apparent viscosity is found at the vertical wall (see Eq. (8)). As shown in the plots of v_a^*, therefore, v_a^* in the localized region of the boundary layers takes a low value of $O(10^{-2})$. This means that the effective viscosity of the fluid is appreciably lower. Consequently, the effective Ra based on v_a, rather than v' (see Eq. (10b)), in the boundary layers increases, being over $O(10^8)$. The transient flow and temperature evolutions are qualitatively similar to the results for a Newtonian fluid for high Ra ($>10^8$) [18]. Fig. 5(a) points to the existence of the short-period oscillations caused by the traveling waves across the boundary layers at early times [17–19]. For $n = 0.8$, the apparent viscosity in the boundary layer is of the order of $O(10^{-1})$ (see the second column in Fig. 5(b)). Therefore, the increase of the effective Ra is rela-

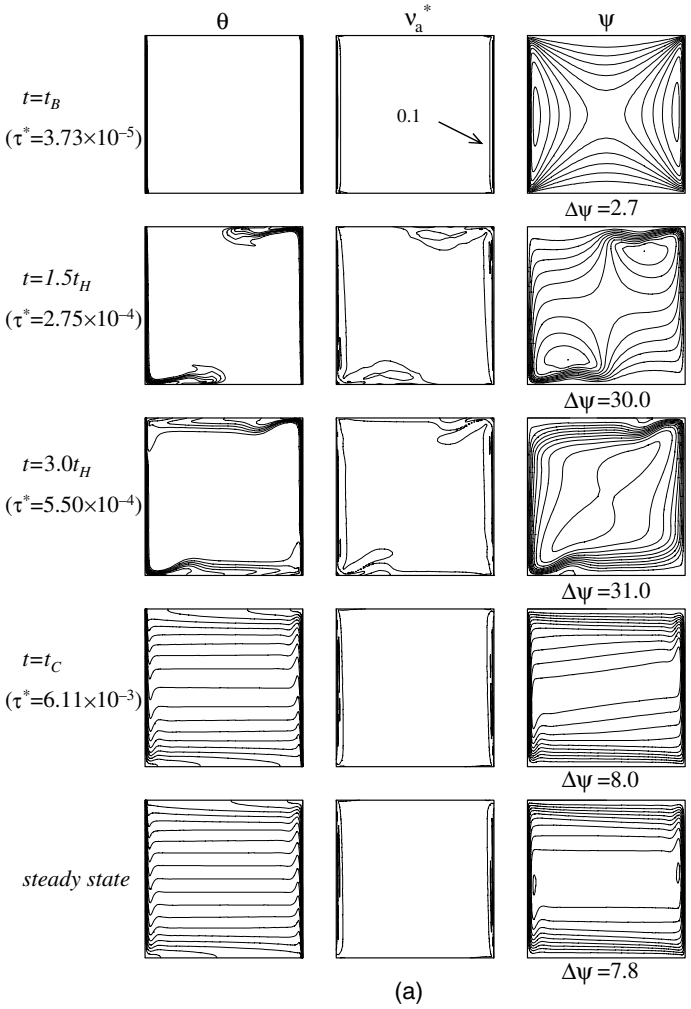

Fig. 5. Evolutions of the temperature (θ), v_a^*, and flow (ψ) fields $Ra = 10^7$, $Pr = 10^2$. (a) $n = 0.6$; (b) $n = 0.8$.

tively small compared with the case of $n = 0.6$, and the flow separation has not been achieved during the intrusion process. The weak counterclockwise eddy is formed near the departing corner in the early stage of intrusion process, but it disappears soon afterward. Most fluids leaving the departing corners are entrained into the opposite wall during the intrusion process. For both cases of $n = 0.6$ and 0.8, at the instant of heat-up time scale ($t = t_C$), the layering by intrusion fills the cavity and the flow becomes substantially horizontal in the core. These features of Fig. 5 are consistent with the previous scalings (see Eqs. (9) and (13)–(17)).

In order to check the validity of the previous scalings, the steady state results are now examined. Fig. 6 exhibits the profiles of the vertical velocity and temperature at the horizontal mid plane ($Y = 0.5$) for $Ra = 10^6$. At low Prandtl number ($Pr = 10^2$), the thickness of the boundary layer becomes thinner and the flow is intensified as n decreases. As Pr increases, the differences in the thickness of the boundary layer and in the flow strength are decreased (see Fig. 6(b)). For a larger value of Pr, a boundary layer-type flow character is pronounced in the Newtonian fluid ($n = 1.0$) (see Fig. 6(c)). For a moderate Prandtl number ($Pr \leqslant O(10^3)$ for $Ra = 10^6$, and $Pr \leqslant O(10^4)$ for $Ra = 10^7$), the power-law index n emerges to be the primary controlling parameter. For an increased value of Pr, the effect of n becomes meager. This feature was also reported in the prior study of Dale and Emery [10] for a flat plate. As pointed out in the previous studies for high Prandtl number, the boundary layer structure of the Newtonian fluid ($n = 1.0$) remains largely unchanged. To the contrary, the results

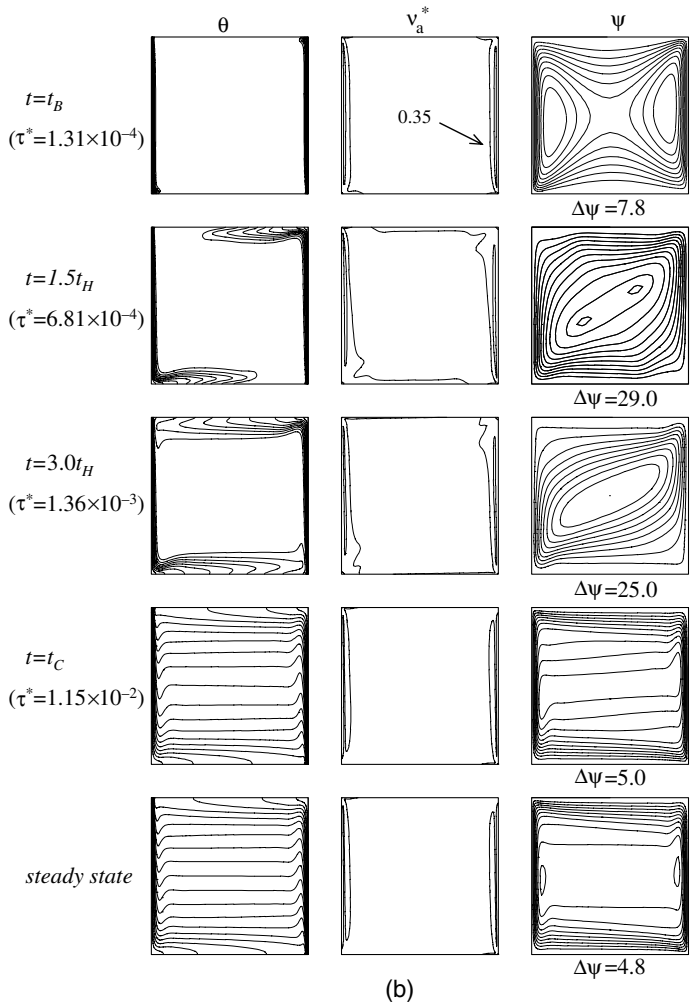

Fig. 5 (*continued*)

of non-Newtonian fluids are dependent on Pr. The lower value of n causes a steeper change with Pr in the boundary layer structure. All these features are supportive of the scalings expressed by Eqs. (11b) and (11c).

Next, by compiling the present numerical data, the variation in the Nusselt number at the steady state, Nu_{ss}, is scrutinized in Fig. 7(a). To investigate the effect of the power-law index n, the Nusselt number for each n is normalized by the corresponding value for a Newtonian fluid ($n = 1.0$). For a high Ra (see the results for $Ra = 10^7$), the augmentation in the overall heat transport for a non-Newtonian fluid, in comparison to the case of a Newtonian fluid, is remarkable [6]. This trend is pronounced at higher Ra and lower n, as demonstrated in Fig. 7(a). Similar results were also observed in the prior studies for a porous cavity saturated with a power-law fluid [12,14]. The effect of Pr is somewhat more complicated. For a non-Newtonian fluid of large Pr (e.g., see the results for $Pr = 10^4$) and low Ra (see, e.g., $Ra = 10^5$), the Nu-values are less than those of the Newtonian fluid. This can be explained by observing the flow character as the apparent viscosity v_a^* is altered. As stressed earlier, the apparent viscosity is flow dependent, and it varies substantially in the cavity. Therefore, the system-wide Rayleigh number and Prandtl number in Eqs. (10a) and (10b) alone may not fully characterize the phenomena. Fig. 7(b) displays the value of the apparent viscosity v_a^* at the vertical wall ($Y = 0.5$). For a boundary layer-type flow configuration, the vertical boundary layer is an active region that induces the buoyant flow, and, therefore, the estimation of v_a^* in this layer is an important task. Fig. 7 reveals that the dependency of the Nusselt number on n is opposite to that of the apparent viscosity v_a^*. Obvi-

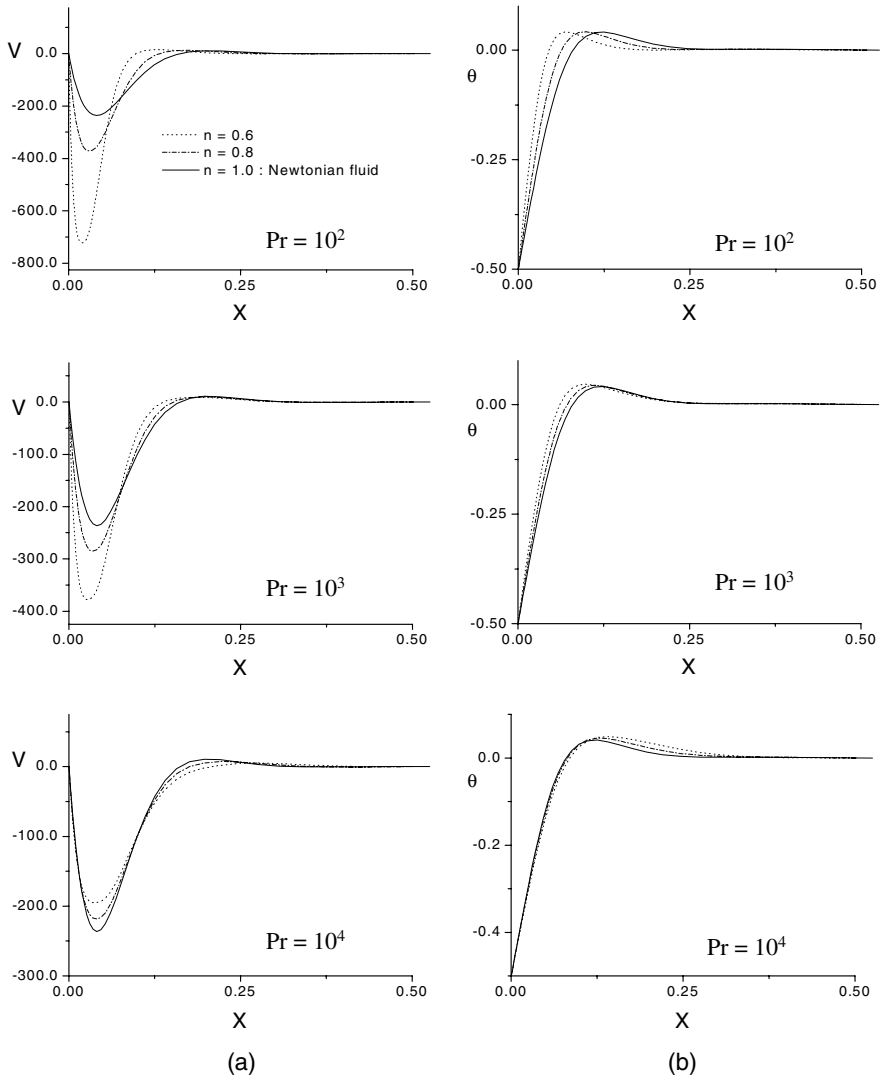

Fig. 6. Horizontal profiles of the vertical velocity (V) and temperature (θ) at the steady state $Y = 0.5$, $Ra = 10^6$. (a) V; (b) θ.

ously, the effective Ra is inversely proportional to the apparent viscosity v_a^*. The effective local Rayleigh number is a measure to gauge the strength of convective activities.

Finally, by recasting the present numerical data for the steady state, the correlation of the Nusselt number is obtained. The heat transfer rate normalized as in Eq. (23) is displayed in Fig. 8. It is clear that the grouping given by Eq. (23) is in broad agreement with the computed results. This combination of flow variables was shown to be effective in depicting the heat transfer enhancement of a non-Newtonian fluid for a flat plate [3,5,6,10]. Considering the dependency on the power-index n, the numerical data of the Nusselt number at the steady state are fitted by curves of the form

$$Nu_{ss} = 0.3n^{0.4}(RaPr^{n-1})^{1/(3n+1)} \tag{26}$$

for $10^6 \leqslant Ra \leqslant 10^7$, $10^2 \leqslant Pr \leqslant 10^4$ and $0.6 \leqslant n \leqslant 1.0$ with a maximum relative error of 6.2%.

6. Concluding remarks

A scaling analysis and comprehensive numerical calculations have been conducted to delineate the features for a purely viscous non-Newtonian power-law

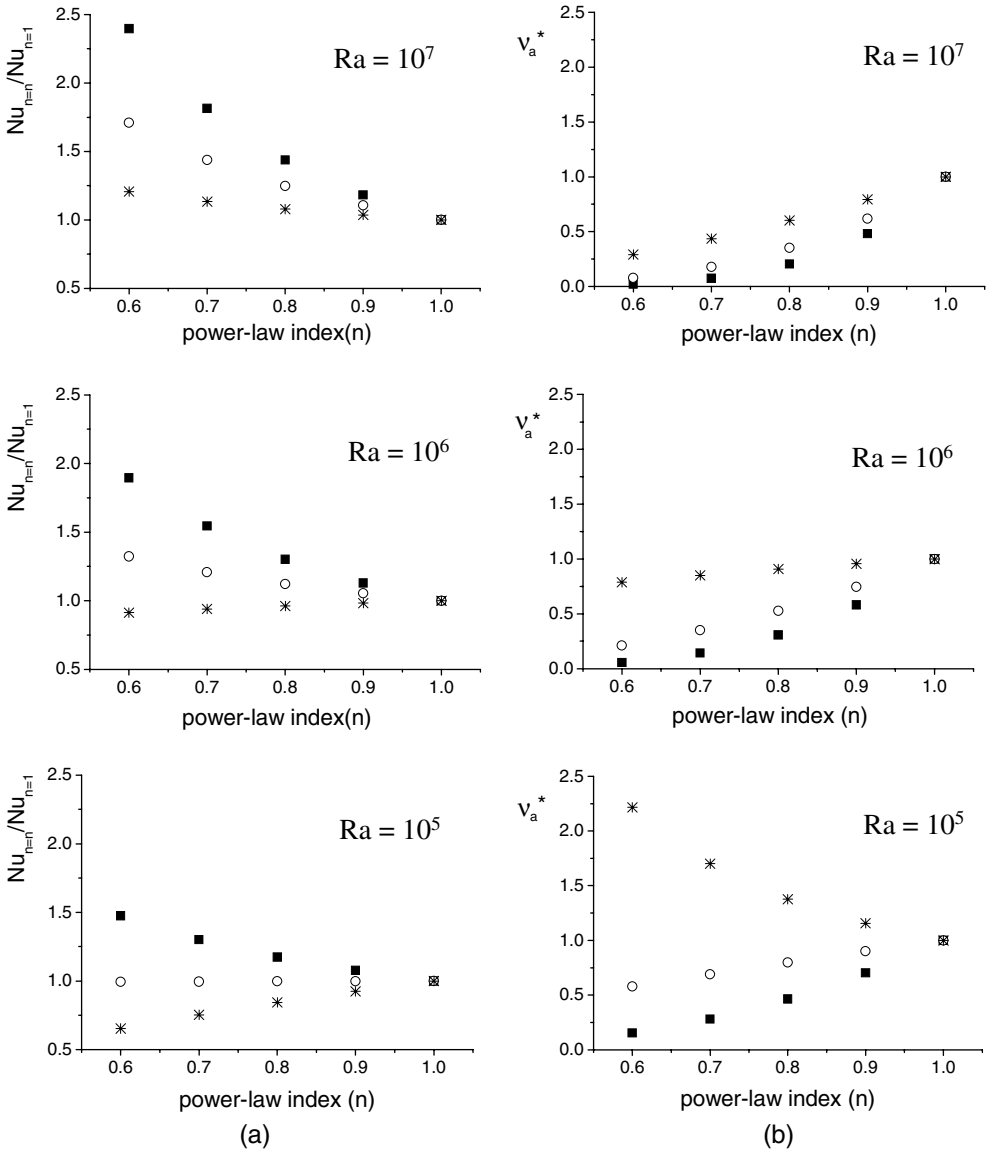

Fig. 7. Variations in the Nusselt number and the apparent viscosity at the steady state. The value of ν_a^* is measured at the vertical wall ($Y = 0.5$). ■: $Pr = 10^2$; ○: $Pr = 10^3$; ✳: $Pr = 10^4$. (a) The Nusselt number; (b) the apparent viscosity.

fluid. The estimations by scaling analysis are shown to be in qualitative agreement with the present numerical results.

The concept of the apparent viscosity (or the apparent Prandtl number) of the non-Newtonian fluid, evaluated in the vertical thermal boundary layer, is a powerful tool. The temporal behavior of *Nu* discloses that the presence of decaying oscillatory motions is anticipated if $Ra > Pr^{(6-2n)/(4-3n)}$ for a shear-thinning fluid ($n < 1.0$). This is in line with the general criterion obtained by the scaling analysis. The period of oscillation is comparable to the period of internal gravity wave. For high *Ra* and moderate *Pr*, as the power-law index *n* decreases, the convective activity is intensified, and the overall heat transfer is enhanced. Consequently, the evolution of flow in the transient process progresses faster. The rheological property has a significant influence on both the transient process and the steady state, and this feature is more pronounced as *Ra* increases and *Pr* decreases.

The correlation of the Nusselt number at the steady state is proposed.

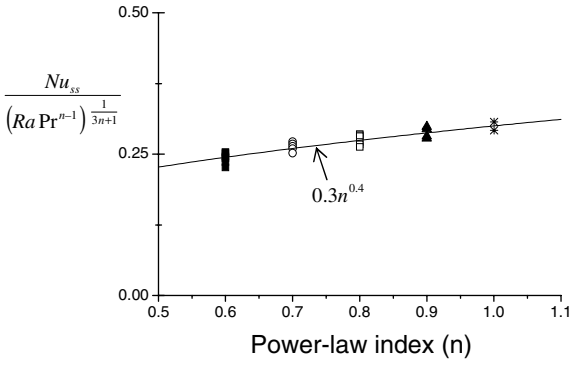

Fig. 8. Computed correlation of the Nusselt number at the steady state $10^6 \leqslant Ra \leqslant 10^7$, $10^2 \leqslant Pr \leqslant 10^4$.

Acknowledgements

Appreciation is extended to the referees for their constructive and helpful comments and suggestions. These led to improvements in the revised paper.

References

[1] J.M. Hyun, Unsteady natural convection in an enclosure, Adv. Heat Transfer 24 (1994) 277–320.
[2] J. Patterson, J. Imberger, Unsteady natural convection in a rectangular cavity, J. Fluid Mech. 100 (1) (1980) 65–86.
[3] A. Acrivos, A theoretical analysis of laminar natural convection heat transfer to non-Newtonian fluids, AIChE J. 6 (1960) 584–590.
[4] S. Haq, C. Kleinstreuer, J.C. Mulligan, Transient free convection of non-Newtonian fluid along a vertical wall, ASME J. Heat Transfer 110 (1988) 604–607.
[5] J.F.T. Pittman, J.F. Richardson, C.P. Sherrard, An experimental study of heat transfer by laminar natural convection between an electrically-heated vertical plate and both Newtonian and non-Newtonian fluids, Int. J. Heat Mass Transfer 42 (1999) 657–671.
[6] A.F. Emery, H.W. Chi, J.D. Dale, Free convection through vertical plane layers of non-Newtonian power law fluids, ASME J. Heat Transfer 93 (2) (1971) 164–171.
[7] T.Y.W. Chen, D.E. Wollersheim, Free convection at a vertical plate with uniform flux condition in non-Newtonian power-law fluids, ASME J. Heat Transfer 95 (1973) 123–124.
[8] A. Som, J.L.S. Chen, Free convection of non-Newtonian fluids over non-isothermal two-dimensional bodies, Int. J. Heat Mass Transfer 27 (1984) 791–794.
[9] Z.P. Shulman, V.I. Baikov, E.A. Zaltsgendler, An approach to prediction of free convection in non-Newtonian fluids, Int. J. Heat Mass Transfer 19 (1976) 1003–1006.
[10] J.D. Dale, A.F. Emery, The free convection of heat from a vertical plate to several non-Newtonian pseudoplastic fluids, ASME J. Heat Transfer 94 (1972) 64–72.
[11] P.Y. Wu, T.J. Liu, H.M. Chang, Natural convection of non-Newtonian liquids in a cylindrical enclosure, Numer. Heat Transfer A 25 (1994) 363–371.
[12] W. Bian, P. Vasseur, E. Bilgen, Boundary-layer analysis for natural convection in a vertical porous layer filled with a non-Newtonian fluid, Int. J. Heat Fluid Flow 15 (6) (1994) 384–391.
[13] W. Bian, P. Vasseur, E. Bilgen, Natural convection of non-Newtonian fluids in an inclined porous layer, Chem. Eng. Commun. 29 (1994) 79–97.
[14] D. Getachew, W.J. Minkowycz, D. Poulikakos, Natural convection in a porous cavity saturated with a non-Newtonian fluid, J. Thermophys. Heat Transfer 10 (4) (1996) 640–651.
[15] S. Paolucci, D.R. Chenoweth, Transition to chaos in a differentially heated vertical cavity, J. Fluid Mech. 201 (1989) 379–410.
[16] J.C. Patterson, On the existence of an oscillatory approach to steady natural convection in cavities, ASME J. Heat Transfer 106 (1984) 104–108.
[17] J.M. Hyun, J.W. Lee, Numerical solutions for transient natural convection in a square cavity with different sidewall temperature, Int. J. Heat Fluid Flow 10 (2) (1989) 146–151.
[18] J.C. Patterson, S.W. Armfield, Transient features of natural convection in a cavity, J. Fluid Mech. 219 (1990) 469–497.
[19] S.G. Schladow, Oscillatory motion in a side-heated cavity, J. Fluid Mech. 213 (1990) 589–610.
[20] W. Schope, J.C. Patterson, Natural convection in a side-heated cavity: visualization of the initial flow features, J. Fluid Mech. 295 (1995) 357–379.
[21] S.V. Patankar, Numerical Heat Transfer and Fluid Flow, McGraw-Hill, 1980.
[22] T. Hayase, J.A.C. Humphery, R. Grief, A consistently formulated QUICK scheme for fast and stable convergence using finite-volume iterative calculation procedures, J. Comput. Phys. 98 (1992) 108–118.